N_2 Active Species in Microwave Plasma and Early Afterglows at Low Gas Pressure

ABSTRACT

The N_2 flowing microwave discharges have been investigated by emission spectroscopy in the following conditions: N_2 at p = 5 Torr, flow rate of 0.3 slpm, t = 1.5×10^{-3} s and microwave power of P = 150 W. The plasma and pink afterglows have been analysed in a setup where the end of the plasma (produced inside a 5 mm ext. dia. tube) was directly connected to a larger post-discharge tube (with a diameter of 15 mm). Under these conditions, the production of N_2^+ ions in the plasma and in the early afterglow is done predominantly by electron collisions. After the end of the plasma up to the pink afterglow, N_2(A) and N_2(X,v>11) were the excited species at the origin of the N_2(C) and N_2^+(B) emissions. A self-consistent theoretical model was introduced to explain the production of the N_2 active species by particle kinetics.
The intensity ratio $I_{N_2^+(B)}/I_{N_2(C)}$ increased 15 times from the plasma to the pink afterglow. In this setup, the gas temperature was about 1000 K in the plasma and 700 K in the pink afterglow. In a second setup, the plasma end was at 12 cm of the post-discharge tube. The gas temperature was lower: 750 K at 2 cm and 400 K at the plasma end (3.5 cm). The effect of adding an Ar-NO_{ext} gas mixture (used for N-atom titration in the late afterglow inside the 15 mm diameter tube) at the discharge end was studied along the 5 mm diameter tube. It was concluded first that the destruction of N-atoms by NO_{ext} decreased the intensity of the N(^{2}P) and N_2(B) radiative states. Second, the electrons at the plasma end could excite the N_2(C) and N_2^+(B) radiative states.

Keywords: Theory of N_2 kinetics, N_2 plasma end, gas temperature, NO interactions.

9.1- INTRODUCTION

The excited states in N_2 plasma and flowing afterglows at reduced pressure are studied in [chap. 1, 6, 2, 4, 10] for the plasmas and in [1, chap. 12-6, 3-9] for the afterglows. After a theoretical analysis of N_2 kinetics reactions which follow electron collisions, it is presently considered the N_2 plasmas and early (pink) afterglows at low gas pressure. Also at the plasma end and before the pink afterglow, it has been analysed the behaviour of N_2 radiative species in interaction with external NO gas, commonly used for N-atom titration in the late afterglow [1, chap. 11].

Two experimental setup was considered. In the first one (setup 1) , the plasma end was at the entrance of the post-discharge tube. In the second one (setup 2) , the plasma end was just before a secondary Ar-NO_{ext} tube used for N-atoms titration. The results obtained with these two setups are successively analysed.

9.2- EXPERIMENTAL SETUP

A photo and schematic representation of the experimental setup of a N_2 microwave plasma and afterglow (setup 1) are presented in Fig 15.1. The right part of the photo shows the surfatron launcher equipped with a 5 mm diameter quartz tube. The plasma of 3.5 cm length has its end placed just at the entrance a 15 mm diameter post-discharge tube.
The left part shows the afterglows in the 15 mm diameter quartz bent tube before a 5 litre reactor where the late afterglow dominates with yellow emission of the N_2, 580 nm band. In the 5 litre reactor a heated sample can be introduced for a surface treatment by N-atoms.

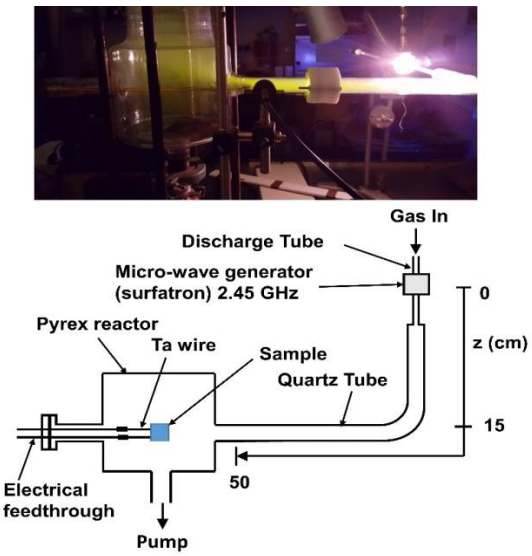

Fig. 9.1. Photo and schematic representation of the setup of a microwave N_2 plasma and afterglow used for surface treatment in a 5 litre reactor. The plasma is produced in a 5 mm dia. quartz tube and the afterglow in a 15 mm dia. quartz tube

High frequency discharges (at 2.45 GHz) are produced using a Surfatron launcher in a quartz tube with 5 mm of internal diameter sealed to a bent quartz tube with an internal diameter of 15 mm. The high frequency power transmitted to the plasma can vary between 30 to 150 watts, with a negligible reflected power.

The total gas flow can be adjusted from 0.1 to 10 slpm and the gas pressure can be adjusted from 0.1 to 50 Torr. The plasma and afterglow lights are collected by a quartz optical fiber connected to a Jobin-Yvon 270M spectrometer (1200 grooves mm-I grating), equipped with a CCD detector.

For the conditions of N_2 pressure p = 5 Torr, flow rate 0.3 slpm and power p = 150 W, the plasma end was at 3.5 cm from the surfatron gap, corresponding to a time of 1.5×10^{-3} s.

9.3 THEORETICAL MODEL

In order to better understand the experimental results, a self-consistent theoretical model is developed for a low-pressure N_2 discharge driven by a propagating surface wave. This model considers the scenario where an azimuthally symmetric (transverse magnetic mode) surface wave propagates along and sustains a N_2 plasma column in a cylindrical dielectric tube, with a permittivity ε_d of 3.71. The z coordinate is directed along the plasma column axis, representing the distance from the gap (see Fig.15.1).

The theoretical formulation comprises a complex system of strongly coupled equations that are simultaneously solved in a self-consistent way. The set of equations encompasses the Boltzmann equation for electrons, rate balance equations for the most important neutral and ionic species in the discharge, equations that describe the vibrational kinetics of ground-state N_2 molecules, gas thermal balance equation, as well as equations that account for wave propagation and power absorption. Together, these equations provide a comprehensive understanding of the processes that occur within the plasma discharge.

For simplicity, we make the assumption that the plasma column is radially homogeneous.
This assumption is reasonable since the focus of this study is on the axial variations in discharge properties, rather than the radial variations. By making this simplification, we can concentrate on the critical aspects of the plasma under investigation without the need to consider unnecessary complexity.

While this approach may introduce some errors in the description of the electron kinetics and wave propagation, it provides a means of dealing self-consistently with the coupling between the discharge kinetic and electrodynamics characteristics.

In the upcoming sections, we will provide a detailed explanation of the system of equations mentioned above, paying special attention to the kinetics of free electrons, electronically excited molecules and charged particles, as well as the kinetics of vibrationally excited nitrogen molecules.

9.3.1 Kinetics of Free Electrons

The electron energy distribution function (EEDF) is obtained by solving the homogeneous electron Boltzmann equation in the local approximation.

The Boltzmann equation is solved using the standard two-term expansion in spherical harmonics [2]. To accomplish this, it is assumed that the anisotropies caused by spatial inhomogeneities and the applied field are small enough to be negligible.

The isotropic part of the distribution function can be considered time-independent since the wave frequency is considered much larger than the characteristic frequency of electron energy relaxation. The collision integral takes into account momentum transfer collisions between electrons and heavy particles, such as N_2 and $N(^4S)$, electron impact excitation of electronic levels of N_2 molecules, $N(^4S)$ atoms, and N_2^+ molecular ions, inelastic and superelastic collisions between electrons and vibrationally excited $N_2(X,v)$ molecules, ionization, stepwise processes, as well as electron–electron and electron–ion collisions. Tables 24.1-4 provide information on the sources and corresponding cross sections for the inelastic and superelastic processes considered.

Table 15.1. Inelastic electron collisions

Number	Process	*k*(cm^3 s^{-1})	Reference
R1	$e + N_2(X,v=0) \rightarrow e + N_2(A, B, C, a', a, w)$	*f*(*E*/*N*)	3
R2	$e + N_2(X,v=0) \rightarrow e + N(^4S)+N(^4S, ^2D)$	*f*(*E*/*N*)	4
R3	$e + N(^4S) \leftrightarrow e + N(^2D, ^2P)$	*f*(*E*/*N*)	5
R4	$e + N_2(X,v=0) \rightarrow N_2^+ + e + e$	*f*(*E*/*N*)	3
R5	$e + N_2(A) \rightarrow N_2^+ + e + e$	*f*(*E*/*N*)	4
R6	$e + N_2(a') \rightarrow N_2^+ + e + e$	*f*(*E*/*N*)	6
R7	$e + N_2(B) \rightarrow N_2^+ + e + e$	*f*(*E*/*N*)	7
R8	$e + N_2^+(X) \rightarrow N_2^+(B) + e + e$	*f*(*E*/*N*)	8

9.3.2 Kinetics of Electronically Excited Molecules and Charged Particles

The model incorporates an extensive range of physical-chemical reactions that govern the populations of electronically excited molecular states, such as $N_2(A,B,C,a',a,w)$ (see Table 15.2), as well as the concentration of the positive ions N_2^+ and N_4^+ (see Table 15.3). N_2^+ ions can be formed via various processes, including electron impact ionization of N_2 molecules, stepwise ionization (see Table 15.1), associative ionization involving $N_2(A)$ and $N_2(a)$ metastables, and charge transfer from N_4^+ ions (see Table 15.3). Similarly, N_4^+ ions can be formed through associative ionization involving $N_2(A)$ and $N_2(a)$ metastables, as well as charge transfer from N_2^+ ions (see Table 15.3). The primary mechanisms for the elimination of charged particles are ambipolar diffusion to the wall and bulk dissociative recombination of N_2^+ and N_4^+ ions. Table 15.3 also includes information on other pathways that contribute to the production or destruction of positive ions.

Table 9.2. Collisional-reactive processes with heavy particles

Number	Process	k(cm^3 s^{-1})	Reference
R1	$N_2(A) + N_2(A) \rightarrow N_2(B) + N_2(X,v=0)$	7.7×10^{-11}	9
R2	$N_2(A) + N_2(A) \rightarrow N_2(C) + N_2(X,v=0)$	1.5×10^{-10}	10
R3	$N_2(A) + N_2 \rightarrow N_2 + N_2$	3×10^{-16}	11
R4	$N_2(B) + N_2 \rightarrow N_2(A) + N_2$	$0.95\times3\times10^{-11}$	12, 13
R5	$N_2(B) + N_2 \rightarrow N_2(X,v=0) + N_2$	$0.05\times3\times10^{-11}$	12
R6	$N_2(C) + N_2 \rightarrow N_2(a) + N_2$	1×10^{-11}	14
R7	$N_2(A) + N_2(X,5\le v\le14) \rightarrow N_2(B) + N_2(X,v=0)$	2×10^{-11}	13, 15
R8	$N_2(A) + N(^4S) \rightarrow N_2(X,6\le v\le9) + N(^2P)$	$4\times10^{-11}\left(\frac{300}{T_g(K)}\right)^{2/3}$	16, 17
R9	$N_2(B) + N_2(X,v\ge12) \rightarrow N_2(C) + N_2(X,v=0)$	1.0×10^{-13}	18
R10	$N_2(a') + N_2 \rightarrow N_2(B) + N_2$	1.9×10^{-13}	19, 20
R11	$N_2(w) + N_2 \rightarrow N_2(a) + N_2$	$0.5\times2.0\times10^{-11}$	21
R12	$N_2(a) + N_2 \rightarrow N_2(a') + N_2$	2.0×10^{-11}	22
R13	$N_2(B) \rightarrow N_2(A) + h\nu$	$\nu = 2\times10^5$ (s^{-1})	15
R14	$N_2(C) \rightarrow N_2(B) + h\nu$	$\nu = 2.74\times10^7$ (s^{-1})	23
R15	$N_2(a) \rightarrow N_2(X,v=0) + h\nu$	$\nu = 1.8\times10^4$ (s^{-1})	22
R16	$N_2(a) \rightarrow N_2(a') + h\nu$	$\nu = 1.91\times10^2$ (s^{-1})	24
R17	$N_2(w) \rightarrow N_2(a) + h\nu$	$\nu = 6.5\times10^2$ (s^{-1})	25
R18	$N(^4S) + N(^4S) + N_2 \rightarrow N_2(X,A) + N_2$	$k_1=8.27\times10^{-34}\exp\left(\frac{500}{T_g(K)}\right)$(cm^6 s^{-1})	20
R19	$N(^4S) + N(^4S) + N_2 \rightarrow N_2(a) + N_2$	$k_2= 5\times10^{-2}\ k_1$	26
R20	Vibrational dissociation, see table 24.1		
R21	$N(^4S) + wall \rightarrow 0.5\ N_2(X,v=0)$	$\gamma=2\times10^{-3}\exp\left(-\frac{1400}{T_w}\right)$	27
R22	$N(^2D, {}^2P) \rightarrow 0.5\ N_2(X,v=0)$		28
R23	$N(^2D, 2P) \rightarrow N(^4S)$		28

Table 15.3. Kinetics of N_2^+ and N_4^+ ions

Number	Process	k(cm^3 s^{-1})	Reference
R1	$N_2(A)+N_2(a') \rightarrow N_4^+ + e$	0.9×10^{-11}	21
R2	$N_2(A)+N_2(a') \rightarrow N_2^+ + N_2(X,v=0) + e$	0.1×10^{-11}	21
R3	$N_2(a')+N_2(a') \rightarrow N_4^+ + e$	$0.9\times5\times10^{-11}$	21
R4	$N_2(a')+N_2(a') \rightarrow N_2^+ + N_2(X,v=0) + e$	$0.1\times5\times10^{-11}$	21
R5	$e + N_2^+ \rightarrow N(^4S) + N(^4S)$	$4.8\times10^{-7}\left(\frac{300}{T_e(K)}\right)^{0.5}$	20
R6	$e + N_4^+ \rightarrow N_2(X,v=0) + N_2(C)$	$2\times10^{-6}\left(\frac{300}{T_e(K)}\right)^{0.5}$	20
R7	$N_4^+ + N_2 \rightarrow N_2^+ + N_2(X,v=0) + N_2$	$2.1\times10^{-16}\exp\left(-\frac{T_g(K)}{121}\right)$	18, 28
R8	$N_2^+ + N_2(X,v=0) + N_2 \rightarrow N_4^+ + N_2$	$6.8\times10^{-29}\left(\frac{300}{T_e(K)}\right)^{1.64}$(cm^6 s^{-1})	29
R9	$N_2(X,v>24)+N_2(a') \rightarrow N_4^+ + e$	1.0×10^{-12}	24
R10	$N_2^+ + N_2(X,v>11) \rightarrow N_2^+(B) + N_2(X,v-12)$	1.0×10^{-11}	30

9.3.3 Kinetics of $N_2(X,v)$ molecules

Table 15.4 shows the list of processes [28,3,21] that were taken into consideration to describe the kinetics of $N_2(X,v)$ molecules. These processes include excitation and de-excitation of vibrational levels by electron impact (e–V), energy exchange involving vibration–vibration (V–V) and vibration–translation (V–T), dissociation and reassociation mechanisms of N_2, and wall deactivation of $N_2(X,v)$ molecules.

Table 9.4. Kinetics of $N_2(X,v)$ molecules

Number	Process	Reference
R1	$e + N_2(X,v) \leftrightarrow N_2(X,w) + e$	3
R2	$N_2(X,v) + N_2(X,w) \leftrightarrow N_2(X,v\text{-}1) + N_2(X,w\text{+}1)$	31
R3	$N_2(X,v) + N_2 \leftrightarrow N_2(X,v\text{-}1) + N_2$	31
R4	$N_2(X,v) + N \leftrightarrow N_2(X,w<v) + N$	32,33
R5	$N_2(X,v) + N \leftrightarrow N + N_2(X,w<v)$	32,33
R6	$N_2(X,v) + wall \rightarrow N_2(X,v\text{-}1)$	3
R7	$e + N_2(X,v) \rightarrow e + N(^4S) + N(^4S)$	4
R8	$N(^4S) + wall \rightarrow 0.5\ N_2(X,v=0)$	3

9.3.4 Gas thermal balance

The theoretical model includes the gas thermal balance equation to account for the energy transferred from the microwave electric field to the plasma electrons, which dissipate this energy through a variety of collisional processes with heavy particles. To simplify the model, we assumed that the gas temperature and velocity have parabolic radial profiles. These profiles are described by the expressions $T(z,r) = 2T_g(z)[1-(r/R)^2]+T_w(z)$ for the gas temperature and $v(z,r) = 2v_0(z)[1-(r/R)^2]$ for the gas velocity. In these expressions, T_g and v_0 denote the radially-averaged gas temperature and velocity, respectively. R is the inner radius of the quartz tube, and $T_w(z)$ is the experimentally measured wall temperature at the axial position z. The thermal balance equation [34] can thus be written as

$$\rho c_p v_0 \frac{\partial T}{\partial z} = v_0 \frac{dp}{dz} - \frac{8\lambda}{R^2}\left(T_g - T_w\right) + \frac{8\mu v_0^2}{R^2} + Q_{in} \qquad (1)$$

where ρ is the mass density and c_p is the average specific heat capacity at constant pressure. On the right-hand side, the first term describes the rate of work done by the pressure per unit volume. The second term describes the power density loss by thermal conduction to the wall, where represents the thermal conductivity of the gas. The third term accounts for the effects of shear viscosity, where represents de viscosity. Finally, Q_{in} accounts for the total net power transferred per unit volume into the translational mode.

The model takes into account several sources of gas heating, including V-V vibrational relaxation of N_2 in N_2-N_2 collisions, V-T relaxation of N_2 in N_2-N_2 and N_2-N collisions, pooling reactions involving $N_2(A) + N_2(A) \rightarrow N_2(X,v) + N_2(B,C)$ reactions, $N_2(X,v)$ vibrational deactivation on the wall, deactivation of $N_2(A,a',a,w)$ metastables molecules at the wall; ion heating involving N_2^+ and N_4^+ ions, and elastic collisions of electrons with neutrals and ions [35].

9.4 - RESULTS BY CONNECTING THE PLASMA END DIRECTLY TO THE POST-DISCHARGE TUBE

With the plasma end just at the entrance of the 15 mm dia.tube , the emission intensity from the N_2,1st positive system between 730 and 790 nm and between 560 and 610 nm are reported in Figs. 24.2 and 24.3, respectively. The emission intensity from the N_2, 2nd positive system and N_2^+, 1st negative system between 360 and 430 nm is shown in Fig. 24.4. The plasma emission was observed in the 5 mm diameter tube for z < 3.5 cm, the pink afterglow was for z = 4-5 cm and the late afterglow for z > 5 cm.

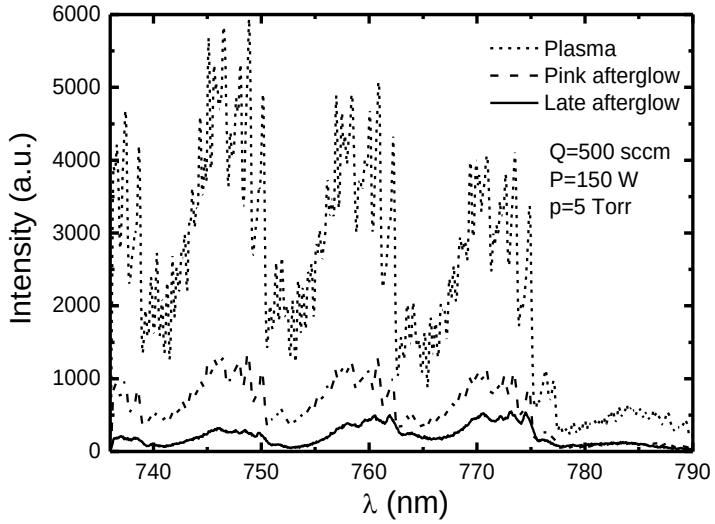

Fig. 9.2. Intensity of the N_2, 1st positive system between 730 and 790 nm in the N_2 plasma for z < 3.5 cm before the 15 mm dia. tube junction and in the pink (z = 4-5 cm) and late afterglows (z > 5 cm)

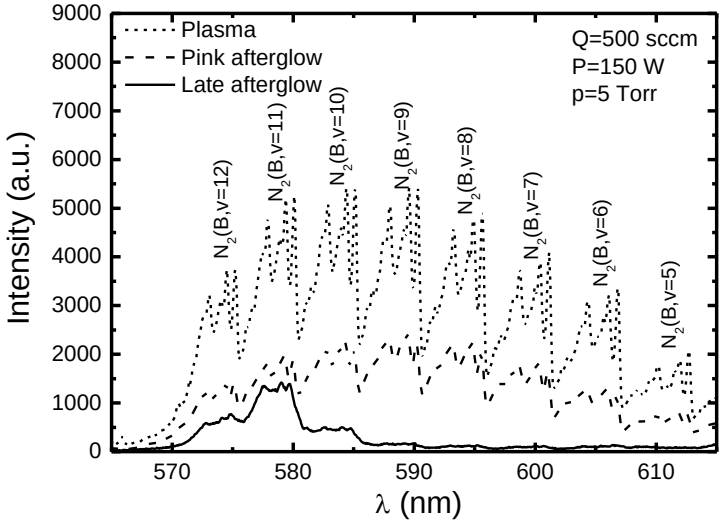

Fig. 9.3. Intensity of the N_2, 1st positive system between 560 and 620 nm in the N_2 plasma for z < 3.5 cm before the 15 mm dia. tube junction and in the pink (z = 4-5 cm) and late afterglows (z > 5 cm)

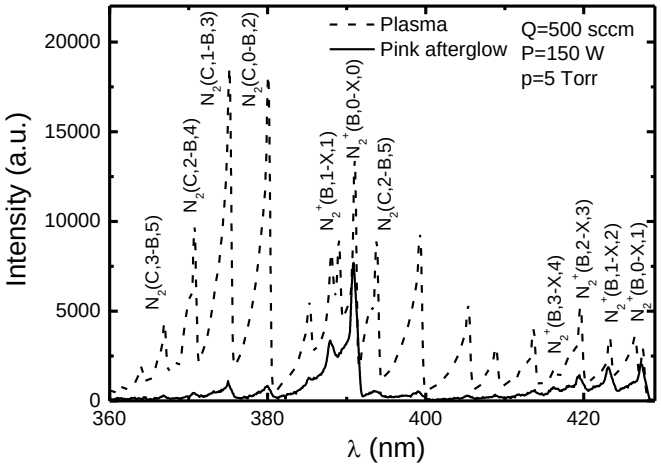

Fig. 9.4. Intensity of the N_2^+, 1st neg. system and N_2, 2nd pos. system between 360 and 430 nm in the N_2 plasma for z < 3.5 cm before the 15 mm dia. tube junction and in the pink (z = 4-5 cm) and late afterglows (z > 5 cm)

By comparing the intensity variations of the bands in Figs. 24.2-4, it can be deduced that, although the intensities of all bands are more intense in the plasma, it is essentially the band intensities from the N_2 (C) state that decrease the most by going from the plasma to the pink afterglow, as opposed to the band intensities from N_2^+(B,0) that remained intense in the pink afterglow (Fig. 24.4).

In the late afterglow the strong emission intensity from the N_2(B,11) state is the signature of the N + N recombination (Fig. 24.3). The atomic nitrogen density at the end of the plasma column is measured by using the N_2 580 nm band intensity after calibration by NO titration [1, chap. 11] in the late afterglow conditions obtained in the 5 litre reactor.

The rotational spectra of the N_2, 1st positive system at 775.3 nm in Fig. 24.2 allows to determine the rotational temperature of N_2 as indicated in [1, chap.1], by measuring the intensity ratio of the P_1/P_2 of the 1st rotational branches.

The variation of the gas temperature T_g versus the axial distance z from the surfatron gap is reproduced in Fig. 24.5.

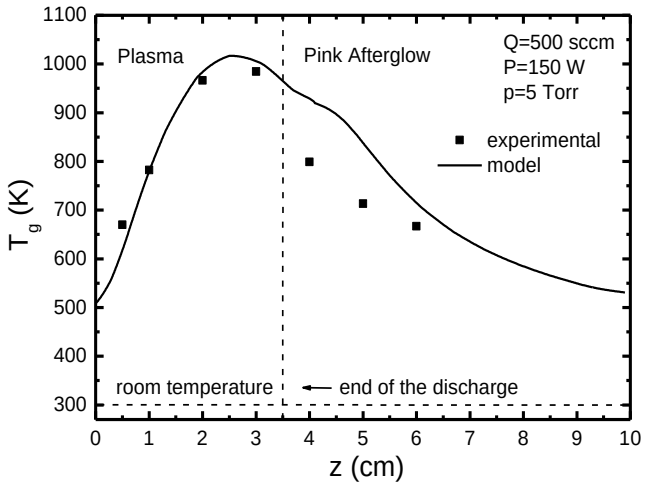

Fig. 9.5. Axial variation of the measured (black squares) and theoretical (solid lines) gas temperature in the plasma and pink afterglow (part 24.3 for the theoretical model)

As shown in Fig. 15.5, the gas temperature increased from 500 K close to the surfatron gap to 1000 K in the middle of the discharge column, remaining almost constant until the end of the plasma. After that, the temperature decreased slightly, attaining 650 K at z = 6 cm.
The results of the calculations (part 15.3) of the relative contribution of the $N_2(C)$, $N_2^+(B)$ and $N_2^+(X)$ production channels (in %) along the axial distance z, for the experimental setup configured in such a way that the plasma end is placed at the entrance of the 15 mm diameter post-discharge tube, are shown in Figs. 15.6, 7 and 8.

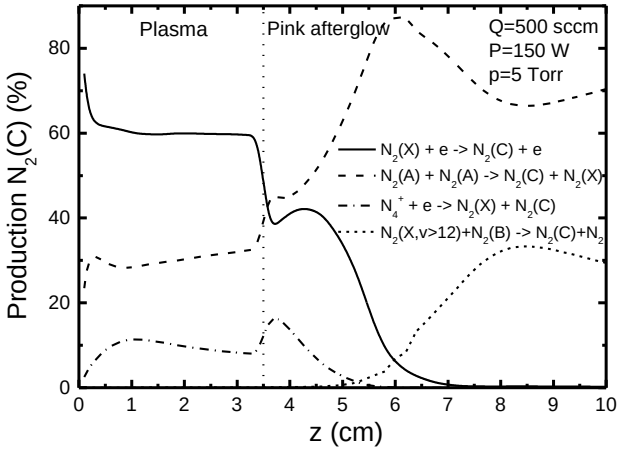

Fig. 9.6. Calculated axial distribution of the relative contribution of $N_2(C)$ production channels (in %) in the plasma and early afterglow

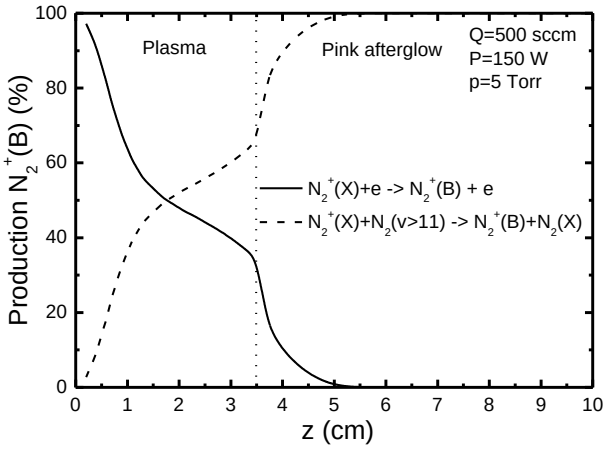

Fig. 9.7. Calculated axial distribution of the relative contribution of $N_2^+(B)$ production channels (in %) in the plasma and early afterglow

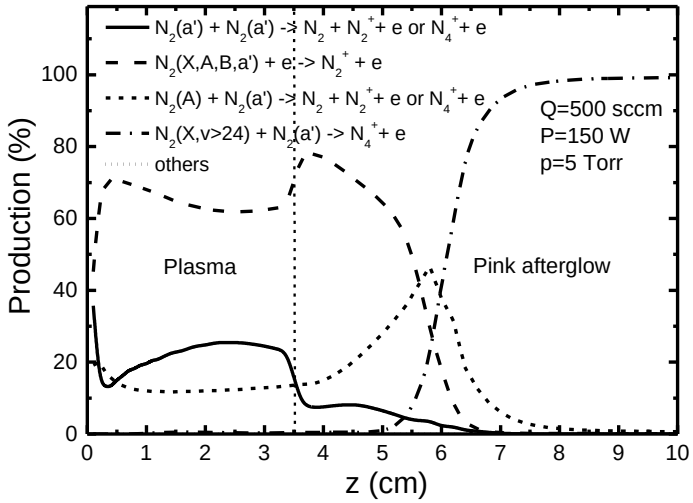

Fig. 9.8. Axial distribution of the relative contribution of N_2^+(N_4^+) production channels (in %) in the plasma and early afterglow

As can be seen in Figs. 9.6 ,7 and 8, it is clear that electronic collisions are the dominant excitation processes in the plasma. But that just after the plasma end, the $N_2(C)$ and $N_2^+(B)$ radiative states are mainly produced by the following reactions:

$$N_2(A) + N_2(A) \rightarrow N_2(C) + N_2(X) \qquad (a)$$

$$N_2^+(X) + N_2(X,v>11) \rightarrow N_2^+(B) + N_2(X) \qquad (b)$$

The N_2^+ ions (Fig. 9.8) are mainly produced by electron collisions in the plasma and after the plasma end up to the pink afterglow. In the pink afterglow, the reactions $N_2(A) + N_2(a')$ and $N_2(X,v>24) + N_2(a')$ are dominant (the $N_2(a')$ state being a metastable state of N_2) .

The intensity ratio between the bands $N_2^+(B,0\text{-}X,0)$ at 391.4 nm over N_2(C,2-B,5) at 394.3 nm is reported in Fig. 9.9. The transition from the plasma to the pink afterglow is clearly demonstrated by a peak of about 15 measured at the axial position z = 5 cm in the 15 mm diameter post-discharge tube, i.e. 1.5 cm after the end of the plasma. By comparison, the same N_2^+, 391.4 nm/N_2, 394.3 nm intensity ratio measured in plasma varies between 1 and 2.

The kinetics modelling of the plasma and early afterglow intensities for z = 0 - 10 cm was in good agreement with the experimental results of Fig. 9.8.

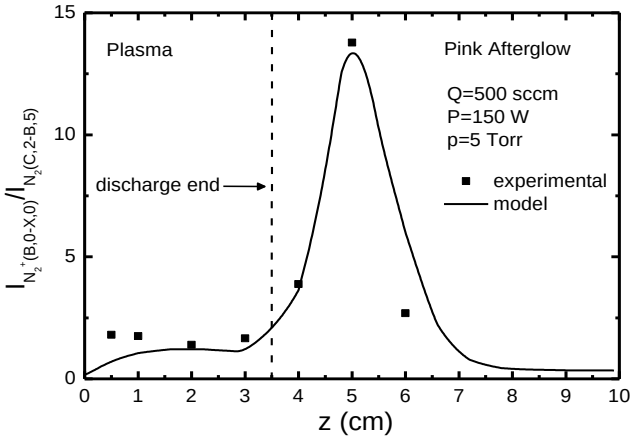

Fig. 9.9. Axial variation of the measured (black squares) and theoretical (solid line) intensity ratio between the bands N_2^+(B,0-X,0) at 391.4 nm and N_2(C,2-B,5) at 394.3 nm in the plasma and pink afterglow

9.5 INTERACTIONS BETWEEN NO_{ext}, INTRODUCED AT THE PLASMA END WITH THE N_2 ACTIVE SPECIES

An experimental schematic representation of the setup arrangement (setup 2) is reproduced in Fig.9.10.

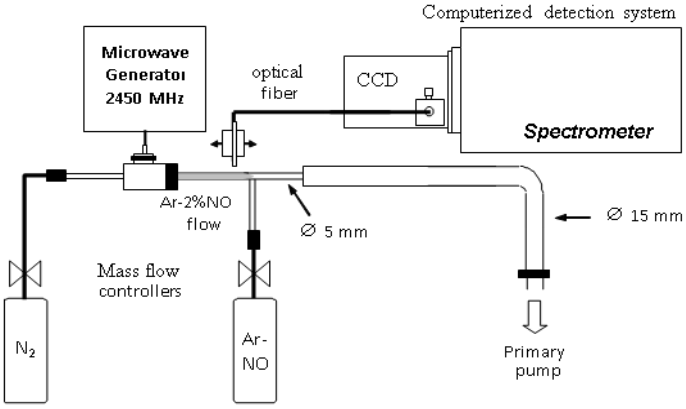

Fig. 9.10. Schematic representation of the experimental setup showing the 2450 MHz surfatron with a 5 mm diameter discharge quartz tube and a 15 mm diameter afterglow tube. An Ar-2%NO flow was introduced at the plasma end (setup 2)

In this experimental setup, an Ar-2%NO_{ext} gas mixture was introduced at the end of the plasma at z = 3.5 cm in the 5 mm diameter tube which was now connected to the 15 mm diameter tube at z=12 cm (setup 2). The NOγ-bands between 200 and 300 nm appeared immediately after the introduction of the Ar-2%NO_{ext} gas mixture at z = 3.5 cm. Such a VUV emission is the result of the reaction of N_2(A) metastable molecules with the externally introduced NO_{ext} as it follows:

$$N_2(A) + NO_{ext} \rightarrow N_2 + NO(A,0) \qquad (c)$$

with a rate coefficient $k_c = 10^{-10}$ cm^3s^{-1} [36].

The N_2(A) density can be obtained by comparing the intensity of the NO(A,0-X,2) transition measured at 247 nm from reaction (c) with the intensity of the N2(B,11-A,7) transition measured at 580 nm from the N+N recombination after titration of N-atom density by NO_{ext} [1 , chap.4].

The I_{247nm}/I_{580nm} intensity ratio is related to the NO(A,0) and N_2(B,11) upper states densities as follows :

$$I_{247\ nm}/I_{580nm} = k_2\ [NO(A,0)]/[N_2(B,11)] \qquad (2)$$

where k_2 was calculated from the $I_{247\ nm}$ and I_{580nm} wavelengths, radiative frequencies and spectral response of the spectrometer.

The spectral response at 247 nm was obtained by comparing the two band intensity from the same N_2(C,2) level: N_2(C,2-B,4) at 371 nm and N_2(C,2-B, 0) at 298 nm and by estimating the same spectral response at 247 and 298 nm. It was found k_2=45.

The N_2(B,11) density was determined from the N-atom density obtained by NO titration in the late afterglow. In conditions of N_2 at 5 Torr (in the 5 litre reactor of Fig. 24.1), Q = 0.3 slpm, P = 150W, it was measured [N] = $7\times10^{14}cm^{-3}$ at the plasma end and then [N_2(B,11)] = $2\times10^{7}cm^{-3}$.

With the introduction of Ar-2%NO_{ext} at a flow rate of 0.12 slpm, it was deduced from eq. 2 a density of [NO(A,0)] = 3×10^{5} cm^{-3}.

From reaction (c), we can deduce that:

$$[NO(A,0] = k_c\,[N_2(A)]\,[NO_{ext}]\ /\ v_R(NOA,0) \qquad (3)$$

In eq. 3, the $v_R(NOA,0)$ radiative frequency being $5\times10^6\ s^{-1}$ [37] is the dominant loss frequency and as $[NO_{ext}] = 10^{15}\ cm^{-3}$, it is calculated $[N_2(A)] = 10^7 cm^{-3}$. The density of $N_2(A)$ is much smaller than that found in [1 , chap.4] in the pink and late afterglows where the densities were in the order of 10^{11} - 10^{12} cm^{-3}. Such a low density at the plasma end is the result of an efficient destruction of $N_2(A)$ by $NO_{ext.}$.

The variations of band intensities from N_2^+ (B,0) , N_2(C,0) , N_2(B,11) and N(^{4}P) with the distance z from the surfatron gap are reproduced in Figs. 15.11a,b,c,d with and without NO_{ext} inlet .

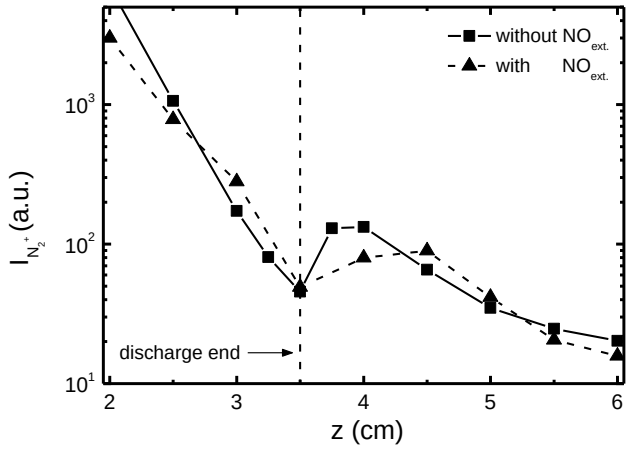

Fig. 9.11a. Axial variation of the intensity of the transition N_2^+(B,0-X,0) at 391.4 nm in the 5 mm diameter tube with and without NO_{ext}. The discharge ends at z = 3.5 cm

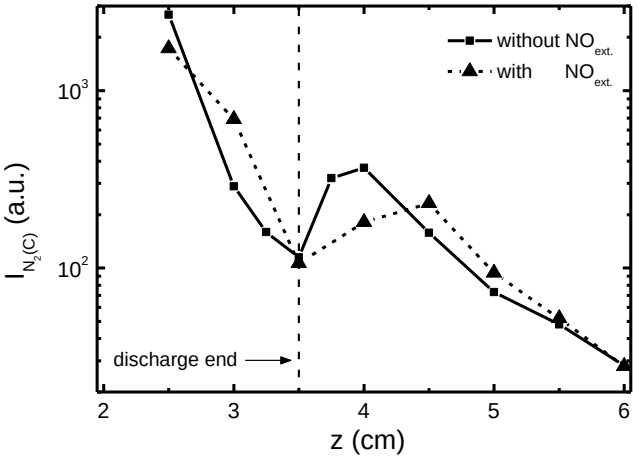

Fig. 9.11b. Axial variation of the intensity of the transition N_2(C,0-B,2) at 380.5 nm in the 5 mm diameter tube with and without NO_{ext}. The discharge ends at z = 3.5 cm

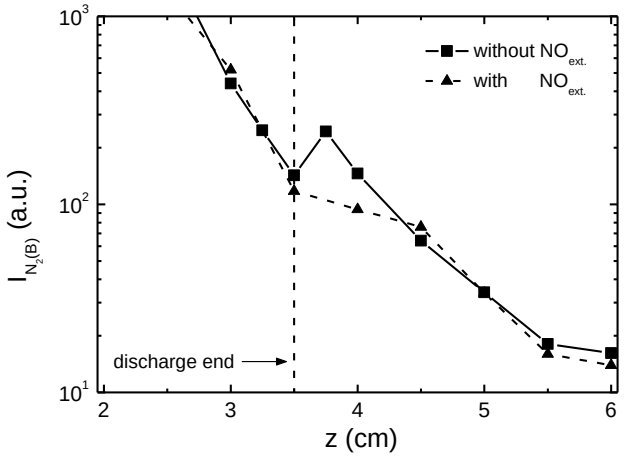

Fig. 9.11c. Axial variation of the intensity of $N_2(B)$ at 777.5 nm in the 5 mm diameter tube with and without NO_{ext}. The discharge ends at z = 3.5 cm

Without NO_{ext}, maximum intensities are observed at z = 4 cm, which are shifted to z = 4.5 cm with NO_{ext} which is correlated to the increase of the flow rate from 0.3 to 0.42 slpm due to the addition of an Ar-2%NO flow rate of 0.12 slpm.

With the setup of Fig. 15.10 (setup 2), the gas temperature decreased from 750 K at z = 2 cm inside the plasma to 400 K at z = 3.5 cm in the plasma end, which is sensibly lower than the temperature measured in the previous setup shown in Fig. 15.1 (setup 1). This variation could be the result of the higher gas pressure inside the 5 mm diameter plasma tube in setup 2, where the plasma end was at 8.5 cm of the 15 mm diameter post-discharge tube, while in setup 1 the plasma end was directly connected to the post-discharge tube.

If the intensity maxima were kept with NO_{ext} for the radiative states of N_2^+(B) and N_2(C), it is not the case for N_2(B) and N(^{4}P) in Fig. 15.11c,d.

At the N_2 plasma end, the high energy electron could excite and ionize N_2 and N to produce the electronic states of Fig 15.11 a,b,c,d.

With NO_{ext}, the N atoms are quickly destroyed by the reaction:

$$N + NO_{ext} \rightarrow N_2 + O \qquad (d)$$

with a rate coefficient of $k_d = 10^{-12}\ (T)^{1/2}\ cm^3s^{-1}$ [37], taking into account that the temperature measured at the plasma end was T = 400 K, we obtain a value of $k_d = 2\times10^{-11}\ cm^3s^{-1}$ at that position.

Reaction (d) can explain the disappearance of the maximum in Fig.15.11d with the N-atom destruction. Also in Fig.15.11c, the disappearance of the maximum of N_2(B) radiative states with NO_{ext} could indicate that these radiative states are produced at the plasma end by N+N atoms recombination as for the late afterglow.

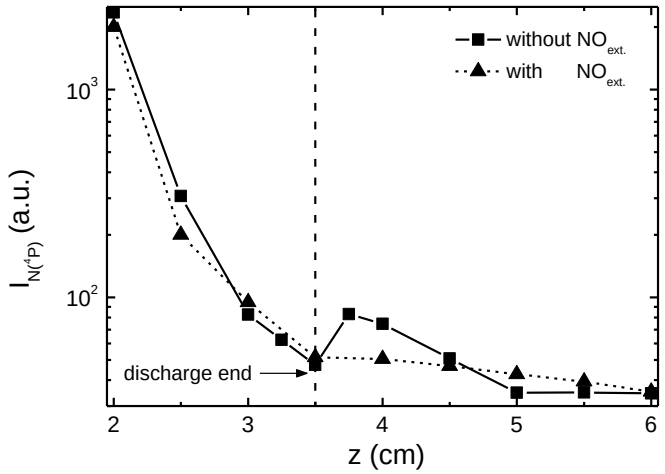

Fig. 9.11d. Axial variation of the intensity of N(^{4}P) at 821.6 nm in the 5 mm diameter tube with and without NO_{ext}. The discharge ends at z = 3.5 cm

As the N_2^+(B) and N_2(C) maxima remained with NO_{ext}, we can conclude that the source of these radiative states are not affected by NO_{ext}.

Since the N_2(A) and N_2^+ species are efficiently destroyed by NO_{ext}, we can conclude that these states are not the source of N_2^+(B) and N_2(C) at the plasma end. If it is assumed that the electron energy is not too much affected by NO_{ext}, it can be estimated that N_2^+(B) and N_2(C) are mainly populated by electron collisions on N_2 molecules as it follows :

$$e + N_2 \rightarrow e + N_2(C) \quad (e)$$

$$e + N_2 \rightarrow e + e + N_2^+(B) \quad (f)$$

and not by the following reactions which are dominant in the pink afterglow :

$$N_2(A) + N_2(A) \rightarrow N_2(C) + N_2 \quad (g)$$

$$N_2(X,v>12) + N_2^+ \rightarrow N_2 + N_2^+(B) \quad (h)$$

9.6 CONCLUSION

The N_2 flowing microwave discharges have been investigated by emission spectroscopy in the following conditions: N_2 at p = 5 Torr, flow rate of 0.3 slpm, microwave power P = 150 W where the plasma end was at z = 3.5 cm from the surfatron gap, corresponding to a time of 1.5×10^{-3} s. The plasma, pink and late afterglows have been analysed in a setup 1 where the plasma end (produced inside a 5 mm diameter tube) was just in front of a large post-discharge tube (with a diameter of 15 mm). A theoretical model including the N_2 electrons collisions, the heavy neutral and ionic particles reactions and a gas thermal balance is detailed. In this condition, the experimental ratio between the intensities of the N_2^+(B,0-X,0) band at 391.4 nm over the N_2(C,2-B,5) band at 394.3 nm increased by a factor of 15 from the plasma to the pink afterglow. In this first setup (setup 1), the gas temperature was about 1000K in the plasma and 700 K in the pink afterglow. In a second setup (setup 2) where the plasma end was at 12 cm of the post-discharge tube, the gas temperature was lower: 750 K at z = 2 cm and 400 K at the plasma end (z = 3.5 cm). In setup 2, the effect of adding an Ar-NO_{ext} gas mixture (used for N-atom titration) at the discharge end was studied along the 5 mm diameter tube.
It was revealed that the destruction of N-atoms caused by the addition of NO_{ext} also produced a decrease in the intensities of the N(^{4}P) and N_2(B) radiative states. The plasma electrons were still influent in the excitation of the N_2(C) and N_2^+(B) radiative states after the plasma end.

REFERENCES

1. A.Ricard (2021, 2022), Plasmas afterglows with N_2 for surface treatments, Bookpi.
2. I. P. Schkarovsky, T. W. Johnston, and M. D. Bachynskii, the Particle Kinetics of Plasmas, Addison–Wesley, Reading, MA (1966).
3. V. Guerra and J. Loureiro, Non-equilibrium coupled kinetics in stationary N_2-O_2 discharges, J. Phys. D 28, 1903 (1995).
4. E. C. Zipf and R. W. McLaughlin, On the dissociation of nitrogen by electron impact and by E.U.V. photo-absorption, Planet. Space Sci. 26, 449 (1978).
5. K. A. Berrington, P. G. Burve, and W. D. Robb, The scattering of electrons by atomic nitrogen, J. Phys. B 8, 2500 (1975).
6. D. Levron and A. V. Phelps, Quenching of $N_2(A^3\Sigma^+_u, v=0,1)$ by N_2, Ar, and H_2, J. Chem. Phys. 69, 2260 (1978).
7. J. Bacri and A. Medani, Electron diatomic molecule weighted total cross section calculation: III. Main inelastic processes for N_2 and N_2^+, Physica B & C 112, 101 (1982).
8. S. De Benedictis, G. Dilecce and M. Simek, Vibrational excitation of $N_2^+(B,v)$ in He-N_2, pulsed RF discharges, J. Phys. B: At. Mol. Opt. Phys. 27 615-632 (1994).
9. L. G. Piper, State-to-state $N_2(A^3\sum^+_u)$ energy pooling reactions. II. The formation and quenching of $N_2(B^3\Pi_g, v'=1–12)$, J. Chem. Phys. 88, 6911 (1988).
10. L. G. Piper, State-to-state $N_2(A^3\Sigma^+_u)$ energy-pooling reactions. I. The formation of $N_2(C^3\Pi_u)$ and the Herman infrared system, J. Chem. Phys. 88, 231 (1988).
11. W. G. Clark and D. W. Sepser, Energy transfer reactions of $N_2(A^3\Sigma^+_u)$ Quenching by hydrogen halides, methyl halides, and other molecules, J. Phys. Chem. 84, 2225 (1980).
12. V.Guerra , E.Tatarova , FM Dias and CM Ferreira (2002) , On the self consistent modeling of a traveling wave sustained nitrogen discharge , J.Applied Phys.91 , 2648
13. L. G. Piper, Energy transfer studies on $N_2(X^1\Sigma^+_g,v)$ and $N_2(B^3\Pi_g)$, J. Chem. Phys. 97, 270 (1992).
14. F. Debal, J. Bretagne, M. Jumet, M. Wautelet, J. P. Dauchot, and M. Hecq, Analysis of DC magnetron discharges in Ar-N_2 gas mixtures. Comparison of a collisional-radiative model with optical emission spectroscopy, Plasma Sources Sci. Technol. 7, 219 (1998).
15. L. G. Piper, The excitation of $N_2(B^3\Pi_g, v=1–12)$ in the reaction between $N_2(A^3\Sigma^+_u)$ and $N_2(X, v\geq5)$, J. Chem. Phys. 91, 864 (1989).
16. L. G. Piper, The excitation of $N(^2P)$ by $N_2(A^3\sum^+_u, v'=0,1)$, J. Chem. Phys. 90, 7087 (1989).
17. M. F. Golde and A. M. Moyle, Study of the products of the reactions of $N_2(A^3\Sigma_u^+)$: The effect of vibrational energy in $N_2(A)$,Chem. Phys. Lett. 117, 375 (1985).
18. D. I. Slovetskii, Mechanisms of Chemical Reactions in Non-equilibrium Plasma Nauka, Moscow, 1980, in Russian.
19. L. G. Piper, Quenching rate coefficients for $N_2(a'^1\Sigma^-_u)$, J. Chem. Phys. 87, 1625 (1987).
20. I.A. Kossyi, A. Yu Kostinsky, A. A. Matveyev, and V. P. Silakov, Kinetic scheme of the non-equilibrium discharge in nitrogen-oxygen mixtures, Plasma Sources Sci. Technol. 1, 207 (1992).
21. P. A. Sá and J. Loureiro, A time-dependent analysis of the nitrogen afterglow in N_2 and N_2 - Ar microwave discharges, J. Phys. D 30, 2320 (1997).
22. W. J. Marinelli, W. J. Kessler, B. D. Green, and W. A. M. Blumberg, Quenching of $N_2(a^1\Pi_g, v'=0)$ by N_2, O_2, CO, CO_2, CH_4, H_2, and Ar, J. Chem. Phys. 90, 2167 (1989).
23. A. Lofthus and P. H. Krupenie, The spectrum of molecular nitrogen, J. Phys. Chem. Ref. Data 6, 113 (1977).
24. R. S. Freund, Radiative Lifetime of $N_2(a^1\Pi_g)$ and the Formation of Metastable $N_2(a'^1\Sigma^-_u)$, J. Chem. Phys. 56, 4344 (1972).
25. M. E. Fraser, W. T. Rawlins, and S. M. Miller, Infrared (2 to 8 μm) fluorescence of the $W^3\Delta_u\rightarrow B^3\Pi_g$ and $w^1\Delta_u\rightarrow a^1\Pi_g$ systems of nitrogen, J. Chem. Phys. 88, 538 (1988).

26. K. H. Becker, E. H. Fink,W. Groth,W. Jud, and D. Kley, N_2 formation in the Lewis-Rayleigh afterglow, Faraday Discuss. Chem. Soc. 53, 35 (1972).
27. Y. C. Kim and M. Boudart, Recombination of oxygen, nitrogen, and hydrogen atoms on silica: kinetics and mechanism, Langmuir 7, 2999 (1991).
28. B. Gordiets, C. M. Ferreira, V. Guerra, J. Loureiro, J. Nahorny, D. Pagnon, M. Touzeau, and M. Vialle, Kinetic model of a low-pressure N_2-O_2 flowing glow discharge, IEEE Trans. Plasma Sci. 23, 750 (1995).
29. H. Bohringer and F. Arnold, Temperature dependence of three-body association reactions from 45 to 400 K. The reactions $N_2^+ + 2N_2 \rightarrow N_4^+ + N_2$ and $O_2^+ + 2O_2 \rightarrow O_4^+ + O_2$, J. Chem. Phys. 77, 5534 (1982).
30. J. Anketell, Cross section for excitation of N_2^+ first negative bands in collisions between ground state N_2^+ ions and vibrationally excited N_2 molecules, Can. J. Phys. 55 1134 (1977).
31. M. Capitelli, C. Gorse, and G. D. Billing, V—V pumping up in non-equilibrium nitrogen: Effects on the dissoviation rate, Chem. Phys. 52, 299 (1980).
32. A. Laganà, E. Garcia, and L. Ciccarelli, Deactivation of vibrationally excited nitrogen molecules by collision with nitrogen atoms, J. Chem. Phys. 91, 312 (1987).
33. I. Armenise, M. Capitelli, E. Garcia, C. Gorse, A. Laganà, and S. Longo, Deactivation dynamics of vibrationally excited nitrogen molecules by nitrogen atoms. Effects on non-equilibrium vibrational distribution and dissociation rates of nitrogen under electrical discharges, Chem. Phys. Lett. 200, 597 (1992).
34. M. J. Pinheiro, B. F. Gordiets and C. M. Ferreira, Modelling of low-pressure surface wave discharges in flowing oxygen: II. Power dissipation and gas heating, Plasma Sources Sci. Technol. 8 31 (1999).
35. J. Henriques, E. Tatarova, V. Guerra and C.M. Ferreira(2002) , Wave Driven N_2-Ar Discharge: I Self-Consistent Model, J. Appl. Phys. 91, page 5622 (2002).
36. LG. Piper , LW.Collins and WT. Rawlins (1986) , State-to-state excitation of NO($A\,^2\Sigma^+$, v'=0,1,2) by N_2($A\,^3\Sigma^+_u$, v'=0,1,2), J.Chem.Phys. 85,3369
37. CD Pintassilgo , J.Loureiro and V.Guerra (2005) , Modelling of a N_2-O_2 flowing afterglow for plasma sterilization , J.Phys.D 38 , 417.
38. J. Henriques, E. Tatarova, F.M. Dias and C.M. Ferreira (2002), Wave Driven N_2-Ar Discharge: II Experiment and Comparison with Theory, J. Appl. Phys. 91, page 5632.
39. J. Henriques, E. Tatarova, V. Guerra and C.M. Ferreira (2003), Nitrogen Dissociation in N_2-Ar Microwave Plasmas, Vacuum 69, pages 177–181.
40. C.M. Ferreira, E. Tatarova, F.M. Dias, V. Guerra, J. Henriques and M. Pinheiro (2003), Wave Driven Molecular Discharges as Sources of Active Species, Vacuum 69, pages 183–187
41. C.M. Ferreira, E. Tatarova, V. Guerra, J. Henriques, B. Gordiets, F.M. Dias and M. Pinheiro (2003), Modelling of Wave Driven Molecular (H_2, N_2, N_2-Ar) Discharges as Atomic Sources, IEEE Trans. on Plasma Sci. 31, pages 645–658.
42. J. Henriques, E. Tatarova, F.M. Dias and C.M. Ferreira, “Spatial Structure of a N_2–Ar Microwave Plasma Source”, J. Appl. Phys 103 103304 (2008). DOI: 10.1063/1.2926551
43. E. Tatarova, F.M. Dias, E.Felizardo, J. Henriques, M.Pinheiro, C.M.Ferreira and B.Gordiets (2010), Microwave Air Plasma Source at Atmospheric Pressure – Experiment and Theory, J. Appl. Phys 108 123305 .
44. J. Henriques, E. Tatarova and C.M.Ferreira (2011), Microwave N_2–Ar Plasma Torch: Modeling, J. Appl. Phys 109, 023301.
45. J. Henriques, E. Tatarova, F.M. Dias, C.M. Ferreira(2014), Microwave N_2 -Ar Plasma Torch, J. Phys.: Conf. Series 516 012004.